Simultaneously improving the corrosion resistance and strength of magnesium via low levels of Zn and Ge additions

R.L. Liu[1], Z.R. Zeng[1], J.R. Scully[2], G. Williams[3], N. Birbilis[1,*]

[1]Department of Materials Science and Engineering, Monash University, Clayton, VIC 3800, Australia
[2]Department of Materials Science and Engineering, University of Virginia, Charlottesville, VA 22904, USA
[3]Materials Research Centre, College of Engineering, Swansea University, Bay Campus, Crymlyn Burrows, Swansea, SA1 8EN, UK

[*] mailto:nick.birbilis@monash.edu

Abstract:

Satisfactory corrosion resistance remains an issue in the widespread implementation of magnesium (Mg). The use of alloying to improve mechanical properties of Mg generally accelerates corrosion due to microstructural heterogeneity. However, recent works have revealed that additions of elements serving as 'cathodic poisons' such as arsenic (As) and germanium (Ge) can reduce cathodic reaction rates and suppress cathodic activation - imparting corrosion resistance. The effect of Ge was translated into a ternary (and mechanically relevant) Mg-alloy system for the first time, revealing an alloy system with a balance of properties, and low rate of corrosion relative to Mg-alloys to date.

Keywords: Magnesium, Magnesium alloys, Zinc, Germanium, Corrosion, Hydrogen evolution, ICP-OES.

1 Introduction

Magnesium (Mg) alloys have the lowest density (~1.74 g/cm^3) of the engineering metals, approximately 65% the density of aluminium alloys and 25% that of steels [1-3]. The high specific strength of Mg alloys makes them attractive materials for the demands of light-weighting in transport and consumer electronics [1-2, 4-5], whilst Mg alloys have also been increasingly studied as biomedical components due to their biocompatibility and bioresorbability [6-7]. Since Mg alloys possess a negative electrode potential in aqueous environments (~ -1.3 to -1.8 V_{SCE}) [8-9], and high theoretical energy density [10-11], they have also been greatly sought for use as electrodes in primary battery systems [12-13].

A high susceptibility to corrosion remains a key issue that restricts the wider commercial utilisation of Mg, including in applications such as the automotive sector [4, 14-16]. The hydrogen evolution reaction, HER ($2H_2O + 2e^- \rightarrow H_2 + 2\ OH^-$), is the primary cathodic reaction in the case of Mg-alloys in aqueous environments, with no kinetic limitation from the requirement of oxygen [11, 17]. Magnesium and its alloys do not nominally possess a protective native oxide/surface layer on their surface in aqueous environments of pH <11, allowing corrosion to readily occur (at high rates) over a large range of pH nominally encountered in service conditions [11, 18]. Uniquely, the HER (a cathodic reaction) can be sustained on the surface of anodically polarised Mg, a phenomenon known as "negative difference effect" (NDE) [19-20]. The NDE has been documented over several decades [5, 19, 21-23]. Recent research regarding the NDE of Mg has also highlighted that anodic dissolution (or anodic polarisation) results in so-called "cathodic activation", whereby the cathodic reaction is catalysed by anodic dissolution of Mg [20-21, 24]. It has also been observed that during exposure aqueous electrolytes at open circuit, hydrogen gas is evolved from the surface of Mg spatially concomitant with the dissolution of Mg [25, 26]; as such, cathodic activation can even occur without external anodic polarisation, allowing the corrosion of Mg to readily proceed (and often accelerate) [19, 20, 27]. Interestingly, it was also recently revealed that such cathodic activation is not unique to Mg, and occurs on many reactive metals including Gd, La and Sc, as shown by Liu [21]. Such a general manifestation of cathodic activation was not unambiguously reported previously, likely due to the fact most reactive metals (other than Mg) with electrode potentials in aqueous electrolytes of << 1V_{SHE} are scarcely used in an engineering context. Interestingly, cathodic activation was empirically associated with metals and electrolytes that have a tendency to form surface hydroxides as the primary surface film [21, 28]. Cathodic activation of Mg impairs several applications of Mg,

such as being the cause of parasitic discharge in Mg primary battery systems [13, 29, 30]. Another salient feature of Mg is that Mg and Mg alloys are non-polarisable or weakly polarisable, manifested by the low "Tafel slope" derived from anodic polarisation testing [19, 31, 32]. Thus, small changes in cathodic kinetics can significantly alter the overall corrosion performance of Mg alloys, placing the corrosion of Mg-alloys under what is termed 'cathodic control'.

The use of alloying, as demonstrated in other metal systems, is one method to impart intrinsic corrosion resistance to Mg. However, unlike the significant improvements realised with mechanical properties, alloying elements generally have either a minor or detrimental effect on the corrosion performance of Mg alloys [19, 31, 33, 34]. The principal reason for this is that Mg is an inherently poor catalyst for supporting the HER (possessing a low exchange current density for HER among all the engineering metals [10, 35]) and thus alloying additions tend to increase the catalytic activity of Mg-alloys. In particular, impurities (such as Fe, Cu and Ni), or second phase particles and intermetallic phases, serve as localised cathodes promoting substantial dissolution of the Mg matrix [31, 36-38]. Furthermore, the limited solid solubility of alloying elements in Mg restricts the possibility of appropriate alloying to form protective oxide films on the surface (such as is done with steels) [31, 39]. An exceptional case was the recent breakthrough of Xu et al.[40], where a bcc structured Mg alloy was produced (by adding >30 at. % Li) and shown to form a Li-rich carbonate film. Such an Mg-Li was revealed to kinetically (as opposed to thermodynamically) provide a significant reduction in corrosion rate [41]. Imparting such a 'stainless' character to other Li-free Mg alloys with an hcp structure remains an important pursuit (as to date, essentially all commercial Mg-alloys are hcp structured).

Following the demonstration that arsenic (As) based compounds could inhibit the corrosion of Mg in aqueous electrolytes [42], Birbilis and co-workers reported an Mg-alloy that contained metallurgically alloyed additions of As (in an Mg-0.37 wt.% As alloy) which demonstrated markedly decreased cathodic kinetics and significantly decreased corrosion rate [43]. The influence of As was attributed to the ability of As to serve as a 'cathodic poison' as it was able to effectively reduce the rate of cathodic HER [35, 42, 44] (as also evidenced by hydrogen collection experiments). However, due to the toxic nature of As, industrial production of Mg-As alloys is complicated due to occupational health and safety considerations [10]. In the pursuit of alloying additions with a cathodic poisoning effect demonstrated by As, more recently, an Mg-0.3 wt.% Ge alloy was developed - capable of

being easily produced without toxicity concerns [45]. On the basis that controlling the rate of anodic kinetics upon Mg by alloying elements which modify surface films is difficult, and that the corrosion of Mg is under the aforementioned 'cathodic control', the use of minor alloying with cathodic poisons such as Ge is a rational means to develop Mg alloys with improved corrosion resistance.

Whilst a binary Mg-Ge has been previously presented with one of the lowest corrosion rates ever reported for an Mg-alloy, it must be noted that requisite mechanical properties are also of great importance in the design of Mg alloys of practical utility. As early as 1942, McDonald investigated the mechanical performance of Mg alloys as a function of Ge alloying content ranging from 0.1 to 10 wt .%, and 0.5~5 wt.% of Ge was suggested to be the optimum range to improve the strength of the alloys [46]. However, the combined mechanical and corrosion performance of ternary Mg-alloys containing Ge (and of which would be of direct relevance to industrial applications) are yet to be reported to date.

Zinc (Zn) has been extensively used as an important alloying addition in the portfolio of the existing Mg alloys, such as the AZ, ZK and ZE series of Mg alloys [1, 31, 47, 48], which also contain either aluminium or zirconium and rare earth additions, respectively. Consequently, there are numerous reports regarding the influence of Zn alloying on the mechanical and corrosion properties of Mg alloys. Hanawalt et al. in 1942 defined a threshold tolerance limit of Zn alloying in Mg of ~ 2.5 wt.% beyond which Zn would rapidly increase corrosion rates [36]. Zinc alloying nominally increases the hardness and tensile strength of Mg alloys, with Kirkland reporting that the addition of Zn (from 1 to 20 wt.%) increased both the compression strength and the yield strength of both binary and ternary Mg-Zn-Ca alloys [6]. As in prior studies, the additional Zn concentration increased the corrosion rate of Mg, where the primary reason for the increase in corrosion rates with excess Zn additions was attributed to both Zn being a better HER catalyst than Mg, and the finding that Mg-Zn intermetallic phases were more noble than the α-Mg matrix, leading to micro-galvanic coupling [6, 38, 47, 49-55]. The strengthening mechanism of Zn alloying was attributed to some grain refinement, in addition to solid solution strengthening and (with further alloying) secondary phase strengthening [56-59]. In addition to the influence of bulk alloy (chemical) composition, several independent studies have also revealed that processing techniques including heat treatment and deformation processing may also optimise microstructure and further improve the mechanical and corrosion properties of Zn containing Mg alloys [47-48, 60-63].

The influence of Ge alloying upon the electrochemical and mechanical properties of Zn containing Mg alloys has not been previously investigated. There is also a lack of information regarding whether Ge in synergy with the Zn additions will affect the HER kinetics and the extent of anodic dissolution induced cathodic activation. Herein, Mg-1Zn (in wt.%) binary alloys, Mg-1Zn-0.3Ge and Mg-1Zn-0.5Ge (in wt.%) ternary alloys were uniquely designed and produced. The alloys were solution treated and extruded to obtain alloys of industrial relevance with regards to processing and properties. The aim of this work was to assess the influence of Ge in combination with Zn additions in order to explore a safe and effective mode of producing Mg alloys with superior corrosion resistance and suitable strength.

2 Experimental procedures

2.1 Materials

The samples used in this work were prepared from commercially pure Mg (sourced from Amac alloys, Australia), pure Zn and pure Ge (sourced from Alfa-Aesar®, USA) with a nominal purity of 99.95 %. Alloys were produced via induction melting using a Leybold-Heraeus ISO1/III induction furnace under a flowing protective atmosphere consisting of Argon and HFC-134a in a ratio of 10:1. The alloy melt was held at 750 ℃ for 30 min in a boron nitride coated steel crucible, while stirred at 6 min intervals to ensure mixing. The molten alloy was cast into a graphite coated and preheated (200 ℃) rectangular steel mould under the same protective atmosphere and allowed to cool to room temperature. The as-cast alloy ingots were subsequently solution treated at 400 ℃ for 24 h and water quenched.

Following solution treatment, the alloys were extruded using a horizontal extrusion press. The extrusion of the alloys was performed at 180 ℃, with an extrusion speed of 1 mm/s and extrusion ratio of 19:1. The alloys were cooled with water following the extrusion process.

The specific chemical compositions of the alloys produced herein are listed in Table 1. The compositions were determined via inductively coupled plasma atomic emission spectroscopy (ICP-AES) by Spectrometer Services (Australia). In all cases, the concentration of the major impurities, such as Fe and Cu were well below so-called impurity threshold values [31, 37]. Trace analysis indicated that the results of this work represent the influence of the selected alloying upon Mg.

2.2 Polarisation experiments

Specimens for potentiodynamic polarisation experiments were mounted within a 45 mm diameter epoxy resin disc. The rear surface of the specimens was connected to a strip of copper tape to provide an electrical connection. For all electrochemical experiments, the surface of the specimens was metallographically prepared to a 1200 grit surface finish by SiC paper. A Biologic® VMP3 potentiostat was used for all the electrochemical testing, under the control of EC-lab 11.10 software. Tests were carried out using a three-electrode electrochemical flat cell (K0235, Princeton Applied Research), with a 1 cm^2 exposed working electrode area, a saturated calomel electrode (SCE) as the reference electrode and a Pt-mesh counter electrode. The test electrolyte herein was quiescent (unbuffered) 0.1 M NaCl in the ambiently aerated condition with ~ 1 atm gas pressure at 25 ℃.

Prior to polarisation experiments, samples were conditioned at open circuit potential (OCP) for 10 min to ensure a relatively stable potential. To fully assess the influence of alloying on the anodic and cathodic kinetics of Mg, separate anodic and cathodic polarisation experiments were carried out. Anodic polarisation was in an anodic or upward scanning direction from 100 mV below OCP to -1 V_{SCE}; whilst cathodic polarisation was performed from 20 mV above OCP to -2 V_{SCE}. The polarisation scan rate was 1 mV/s.

A custom galvanostatic-potentiostatic electrochemical signal was applied to further assess the cathodic activity of the specimens following anodic polarisation. The testing signals involved cyclic anodic polarisation in a stepwise increasing manner from 0.025 to 2.5 mA/cm^2 with a 2 min duration for each step. Potentiostatic currents at a fixed negative potential, -2 V_{SCE} were hold between each anodic current step to measure the cathodic current density sustained upon the anodically polarised surface. The galvanostatic-potentiostatic experiments were repeated with higher anodic polarisation current density (2~24 mA/cm^2) for a comprehensive analysis. This technique has been shown to provide quantitative information to evaluate the extent of anodic polarisation induced cathodic activation of Mg [21, 24, 27].

2.3 Mass loss and hydrogen collection

The mass loss and hydrogen collection testing were performed to assess the longer term cumulative corrosion of specimens. The procedures for the preparation and cleaning of immersion test specimens were in accordance with the ASTM-G1-03 standard [64]. All specimens were prepared from the extruded alloys and metallographically machined into cuboids with an exposed surface area of approximately 5 cm^2. The surfaces of the specimens were ground to 1200 grit finish by SiC paper and cleaned with ethanol. Prior to the immersion testing, the dimensions and weight of all the specimens were accurately measured. The tests were carried out in 0.1 M NaCl over a 24 h duration in quiescent and ambiently aerated conditions at 25 ℃. An inverted burette and funnel set up were utilised to collect the hydrogen gas evolved from the specimens during the immersion. Following immersion testing, specimens were cleaned by chromic acid solution (200 g/L chromium trioxide, 10 g/L silver nitrate and 20 g/L barium nitrate) to remove surface corrosion products prior to the weighing of the specimens.

2.4 Microstructural analysis

Microstructural analysis of the samples was conducted using a JEOL 7001F scanning electron microscope (SEM) equipped with a Bruker energy dispersive x-ray spectroscopy (EDXS) detector, in backscattered electron (BSE) mode. SEM samples were metallographically polished to a 0.05 μm surface finish using a silica suspension and rinsed with ethanol.

The characterisation of corrosion morphologies following 24 h immersion in 0.1 M NaCl was carried out by SEM in secondary electron (SE) mode. Prior to the SEM imaging, the corroded specimens were cleaned by chromium acid solution to remove the corrosion products.

Grain size characterisation of the specimens was performed using an FEI® Quanta 3D-FEG dual beam scanning electron microscope equipped with a Pegasus Hikari® electron backscattered diffraction (EBSD) detector. TSL-OIM 6 software was used for the analysis of EBSD results. The size of grain was calculated from the measurement of grain area and represented in the form of grain size diameter ($\sqrt[2]{\frac{Grain\ area}{\pi}}$).

2.5 Atomic emission spectroelectrochemistry (AESEC)

Atomic emission spectroelectrochemistry experiments were carried out for the quantitative analysis of the dissolution rates of Mg at OCP and polarised conditions. This AESEC method as developed by Ogle has been demonstrated to have ultra-sensitivity in detecting dissolved metal ions as a result of free corrosion or dissolution in response to electrochemical polarisation [65-69]. An electrochemical flow cell coupled with an Inductively Coupled Plasma-Optical Emission Spectrometer (ICP-OES) was utilised in the experiment. The flow cell (012799, ALS Co.) was used in a three-electrode configuration with an exposed working electrode area of 0.6 cm^2. The 0.1 M NaCl electrolyte was continuously pumped through the flow cell tubing at a flow rate of 1 ml/min. The downstream electrolyte from the flow cell was carried to the coupled ICP-OES instrument for instantaneous analysis of dissolved metal ions. A Perkin Elmer® Optima 8000 ICP-OES spectrometer controlled by Syngistix software was used in this experiment. The emission wavelength for the detection of Mg is 279.07 nm with a detection limit of ~ 1 ppb.

The electrochemical control of the AESEC experiment was controlled by a Bio-logic® SP150 potentiostat. Potentiodynamic polarisation was carried out after 10 min exposure to the flowing electrolyte at the OCP. The polarisation testing was commenced from -100 mV below OCP to -1V_{SCE} at a scan rate of 1 mV/s. The dissolved Mg^{2+} ion concentration was measured

as a function of time by the means of ICP-OES and converted to the partial elemental dissolution current density (i_{Mg}^{2+}) using the Faraday's law, by equation (1) [27, 67]:

$$i_{Mg}^{2+} = n.F.f.C_M / A \quad (1)$$

Where n is the oxidation state of the dissolved ions (n = 2 for Mg), F is the Faraday's constant, f is the flow rate (f = 1 ml/s), C_M is the volume adjusted ion concentration and A is the exposed working electrode surface area (A = 0.6 cm^2).

2.6 Microhardness and tensile testing

Microhardness testing was performed on all extruded Mg alloy samples. Prior to the testing, samples were metallographically prepared to a 1200 grit SiC paper surface finish and ultrasonically cleaned in ethanol. An auto-harness tester (Struers® Duramin A300) was used for the microhardness testing with a 1kg load. Ten measurements were performed on each sample.

Tensile testing was performed on specimens were prepared from the Mg alloy extrusions with a gauge length of 10 mm and a width of 5 mm. An Instron® 4505 tensile test machine was used in all testing, with tests carried out at 25 ℃ with an initial strain rate of 0.001 /s.

3 Result and Discussion

3.1 Microstructural analysis

The microstructures of the alloys prepared herein were analysed by backscattered electron imaging in conjunction with EDX mapping, as shown in Fig. 1.

The microstructure of the Mg-Zn alloy consisted of a single α-Mg phase, with Zn alloying homogenously distributed in the matrix with no obvious solute segregation (Fig. 1a). Conversely, with Ge additions (0.3~0.5 wt.%) to Mg-Zn, the presence of additional intermetallic particles was stimulated in the microstructure, as evident by the particles of brighter contrast in BSE-SEM images (Fig. 1b and 1c). The notable microstructure difference between Ge free and Ge containing Mg-Zn alloys is due to the relatively high solid solubility of Zn (maximum ~2.5 at.%) and limited solid solubility of Ge in Mg (which is reported to be ~0.003 at.% at 602 ℃) [70]. The microstructure of Mg-Zn-Ge alloys reveals the presence of intermetallic particles with a columnar morphology in the α-Mg matrix. Energy dispersive X-ray spectroscopy revealed that intermetallic phases in Mg-Zn-Ge alloys contained principally elemental Ge and Mg. There was no evidence that Zn (which is present in the α-Mg matrix) was associated with second phase/intermetallic particles. It is noted that there is a paucity of thermodynamic data available for the prediction of equilibrium phase in Mg-Zn-Ge alloys (i.e. using PANDAT® or ThermalCalc® Mg databases). The stoichiometry of the Mg-Ge intermetallic phase in Mg-Zn-Ge alloys is posited to be Mg_2Ge, as in the case of Mg-Ge binary alloy [21].

Grain size determination of the alloys tested herein was carried out using EBSD mapping, as presented in Fig. 2. It was observed that the average grain size of the extruded Mg-1Zn alloy was ~1.2 μm. The grain structure of the Mg-Zn alloy was revealed to be uniform in grain size and shape. A large fraction (~85 %) of α-Mg grains were equiaxed ranging from ~0.6 to 3.2 μm in grain size dimension (Fig. 2a). In the case of Mg-Zn-Ge alloys, a bimodal grain size distribution was observed suggesting that ternary alloying additions of Ge could alter the grain size distribution of the Mg-Zn alloy. It was observed that the microstructure of extruded Mg-Zn-Ge alloys contained several discrete columnar grains (larger than 10 μm) (Fig 2b and c). The fraction of the large columnar grains increased with Ge concentration from ~1 % to ~16 % (Fig. 2d).

3.2 Potentiodynamic polarisation experiments

Potentiodynamic polarisation tests were performed in quintuplicate and the typical polarisation curves and presented in Fig. 3 for the three distinct alloys studied herein.

The potentiodynamic polarisation response of pure Mg was also included for the purposes of electrochemical assessment, as it represents a reference point of zero alloying additions for comparison purposes. It can be observed from Fig. 3 that binary alloying additions of Zn increased the corrosion potential (E_{corr}) of pure Mg by ~50 mV. The ternary alloying addition of Ge decreased E_{corr} (of Mg-Zn) by ~90mV (to ~ -1.67 V_{SCE}).

It can be observed that the alloys produced herein (both Mg-Zn and Mg-Zn-Ge) demonstrated similar behaviour on the anodic polarisation responses compared to that of pure Mg (Fig. 3), suggesting a minor influence of alloying on the anodic kinetics of Mg. As such, the changes in E_{corr} observed were nominally from alteration of cathodic kinetics, influenced by alloying. To further elucidate the influences of the alloying on the cathodic kinetics of Mg, cathodic potentiodynamic polarisation was carried out (Fig 4).

It is revealed in Fig. 4 (which also includes polarisation data from Pure Mg as the benchmark for comparison) that the Mg-Zn alloy exhibited a higher rate of cathodic reaction than that of pure Mg; with Zn enhancing cathodic (HER) kinetics. In contrast, ternary additions of Ge shifted the cathodic polarisation response to lower current densities (for the case of Mg-Zn-Ge), indicating that the addition of Ge to Mg-Zn alloys supersedes the effect of Zn alloying - significantly decreasing the HER kinetics.

3.3 Mass loss and hydrogen collection tests

Whilst potentiodynamic polarisation reveals the relative anodic and cathodic kinetics of the alloys produced herein, due to the instantaneous nature of polarisation experiments [71], longer-term exposure testing at open circuit potential (OCP) was performed to assess the corrosion behaviour of the alloys under investigation. Testing over a longer period was carried out in 0.1 M NaCl, using a 24 h immersion period. The summary of mass loss and hydrogen evolution is presented in Fig. 5, with pure Mg included for comparison.

It can be seen from Fig. 5 that ternary additions of Ge and Zn decreased the corrosion rate of Mg, as indicated by the lower extent of mass lost following exposure testing - compared with that of pure Mg and Mg-Zn alloy. In agreement, the attendant hydrogen gas evolved from the Mg-Zn-Ge alloy was also lower. Concomitantly, a lower rate of mass loss and hydrogen evolution was realised for the Mg-Zn-Ge alloys. The results of mass loss and hydrogen

collection reveal the ability of combined additions of Zn and Ge to decrease the corrosion rate of Mg.

Scanning electron micrographs in secondary electron (SE) mode of the surface morphology (following chromic acid cleaning) for alloys produced herein and pure Mg are presented in Fig 6.

A typical filiform-like corrosion morphology was observed on the surface of pure Mg and the Mg-Zn alloy (Fig. 6a and 6b). The presence of such filiform like corrosion has been reported to be associated with the enhanced catalytic ability of the Mg surface previously anodically dissolved, towards HER [22, 72]. The corrosion morphology observed upon the surface of Ge containing alloys (with both 0.3 and 0.5 wt.% Ge) is present in the form of discrete superficial corrosion sites (Fig. 6c and 6d). The difference in corrosion morphology (which is noted to be cathodically controlled) was ascribed to the functionality of Ge alloying to suppress both the cathodic kinetics and cathodic activation of Mg.

3.4 Response of galvanostatic-potentiostatic experiment for assessment of cathodic activation

The galvanostatic-potentiostatic experiment was carried out to assess the effects of alloying on the cathodic activation of Mg. The abridged results are presented in Fig. 7. Pure Mg was also benchmarked against alloys produced herein.

Fig. 7a summarises the results of tested specimens with anodic dissolution current density from 0.025 to 2.5 mA/cm^2. It can be seen from Fig. 7 that cathodic current density gradually increased with increasing anodic dissolution current density for all tested specimens, suggestive of enhanced rate of cathodic reaction arising from prior anodic polarisation. It was also noteworthy that the magnitude of cathodic current sustained upon Mg-Zn-Ge alloys was about 2~3 times lower than that of the Mg-Zn alloy and pure Mg irrespective of the level of prior anodic dissolution. This slower rate of cathodic reaction reveals the beneficial effects of Ge additions to suppress the cathodic kinetics and cathodic activation following anodic polarisation for both Mg-Zn alloy and pure Mg.

The galvanostatic-potentiostatic experiment was further carried out to assess the response of tested specimens with higher anodic dissolution current density from 2 to 24 mA/cm^2, as shown in Fig. 7b. A similar trend was observed, whereby all tested specimens displayed

evident cathodic activation following anodic polarisation. Whilst, markedly lower cathodic current was observed for the alloys with Ge additions, it was also noted that the Mg-Zn alloy exhibited relatively lower cathodic current in comparison to that of pure Mg. Such an observation might not have been expected, based on the results of cathodic polarisation. The possible reason for this is that both corrosion rate and cathodic activation of Mg is a time-dependent process and that the influence of Zn alloying on the cathodic kinetics of Mg is not fully revealed, especially over the short duration of the potentiodynamic experiments represented in Figure 4.

3.5 AESEC analysis of the Mg-Zn-Ge alloys

Atomic emission spectroelectrochemisrty testing of the Mg-Zn-Ge alloys was carried out in order to further rationalise the mechanistic role of alloying additions upon dissolution. The Mg dissolution current density (i_{Mg}^{2+}) determined by online ICP-OES analysis during the open circuit potential (OCP) and potentiodynamic polarisation exposure for pure Mg and the Mg alloys produced herein in 0.1 M NaCl is presented in Fig 8. Again, pure Mg was included as a benchmark.

It is observed immediately from the visual inspection of Fig. 8a that a rapid and instantaneous dissolution of Mg commenced from initial few seconds of exposure of the electrolyte and then stabilised with a steady dissolution rate at OCP for all tested specimens. Such rapid attainment of steady dissolution rate was attributed to the low resistance of the metal-electrolyte interface, which indicated the dynamic development of so-called "temporarily protective hydroxides films", as previously reported by Williams and co-workers [25]. Following a 10 min OCP conditioning, potentiodynamic polarisation was carried out from 100 mV below OCP to -1 V_{SCE} with a 1 mV/s scanning speed. It was observed that persistent dissolution of Mg occurred during cathodic polarisation for all tested specimens. This unsuppressed dissolution of Mg under low cathodic overpotential (with respect to OCP) has also been noted by other independent studies [41, 73]. Upon transition to anodic polarisation, i_{Mg}^{2+} commenced to increase gradually with exposure time. Another salient feature of the data in Fig. 8a is that a relatively lower value of i_{Mg}^{2+} was realised with combined additions of Zn and Ge during OCP and potentiodynamic polarisation exposure. The AESEC results reveal that binary additions of Zn had a small impact on the anodic kinetics of Mg; whilst the ternary

Ge alloying additions to the Mg-Zn alloy decreased the anodic dissolution rate of the alloy, both at OCP and during anodic polarisation.

The potentiodynamic polarisation data collected by AESEC analysis is presented in the format of applied potential vs. current density i_{Mg}^{2+} (in logarithmic form), as shown in Fig. 8b. It can be seen from Fig. 8b that, the dissolution current density, i_{Mg}^{2+} increased linearly on the log scale with increasing potential for all tested specimens, representing the nominal "Tafel behaviour". The magnitude of the anodic partial reaction current density of Mg-Zn-Ge alloys was markedly lower compared to that of pure Mg and the Mg-Zn alloy. This is suggestive of the ability of Ge alloying to reduce the anodic kinetics of the Mg-Zn alloy and pure Mg independent of cathodic partial reaction, as ICP determined i_{Mg}^{2+} was only associated with the anodic partial reaction [74]. However, the ICP determined data (Fig. 8b) is somewhat different from that of conventional electrochemical testing (Fig. 2).

3.6 Microhardness results

Microhardness testing was carried out to evaluate the hardness of the alloys produced herein, the results of which are presented in Fig. 9a.

It can be seen from Fig. 9a that the hardness of the Mg alloys was increased with increasing alloying content, from ~50 HV_1 for the extruded Mg-1Zn alloy to ~83 HV_1 for the extruded Mg-1Zn-0.5Ge alloy.

3.7 Tensile testing results

Tensile tests were performed to evaluate the tensile properties (yield strength and ductility) of the Mg-Zn-Ge and Mg-Zn alloys produced herein; the results of which are shown in Fig. 9b.

The extruded Mg-1Zn alloy possessed a yield strength (YS) of ~257 MPa, with a total elongation of ~23%. However, with the addition of 0.3 wt.% Ge to the Mg-1Zn alloy, the yield strength of the alloy increased to 281 MPa, with an attendant 5% reduction in elongation. Further increasing ternary Ge alloying content to 0.5 wt.%, the yield strength of the Mg-Zn-Ge alloy increased to ~311 MPa, whilst total elongation decreased to ~16%.

The increase in both the hardness and yield strength was attributed to the presence of the Mg_2Ge phase (the phase appearing to be a strengthening phase) and the bimodal grain size distribution of Mg-Zn-Ge alloys (allowing an increase in strength owing to the Hall-Petch effect [75, 76]). The reduction of ductility with increasing Ge content (0.3~0.5 wt.%) indicates that there is a trade-off between the strength and ductility of the alloys produced and

studied herein. However, it is noted that the tensile strength of the (extruded) Mg-Zn-Ge alloys herein is considered exceptionally high in the context of specific strength displayed by Mg-alloys (noting that the alloying concentrations studied in this work are considered dilute). Furthermore, the accompanying ductility is also considered to be significant. As a comparison, Mg alloy AZ31 has the following properties YS= 229 MPa, total elongation = 15 %, AZ91 YS = 264 MPa, total elongation = 9 %, and WE43 YS= 237 MPa, total elongation = 16 %, as some examples [2, 77-79]. Indeed, the optimisation of alloying concentration in the Mg-Zn-Ge system, to balance strength, ductility, and corrosion resistance, remains important future work.

3.8 General discussion

Mg-Zn-Ge alloys displayed significantly reduced corrosion rates in comparison to that of pure Mg and Mg-Zn (Fig. 5). The results were rationalised on the basis of potentiodynamic polarisation tests combined with longer-term observations from mass loss and hydrogen collection. The corrosion morphology following immersion testing was also considerably altered by combined alloying additions of Zn and Ge, from heavily corroded filiform-like corrosion attack to discrete superficial corrosion sites (Fig. 6).

The AESEC testing herein provided some unique insights, revealing the influence of alloying on the kinetics of the anodic partial reaction of Mg. This was rationalised on the basis that AESEC determined dissolution current (i_{Mg}^{2+}) is only associated with the anodic partial reaction, irrespective of other effects such as cathodic activation - which cannot be isolated from net current measurements by a potentiostat. It is noticeable that the values of AESEC determined current densities from potentiodynamic polarisation were as much as an order of magnitude lower than those measured by the potentiostat. This indicates that ion concentration (Mg^{2+}) detected by ICP-OES did not represent all dissolved ions; whilst a large fraction of dissolved ions (Mg^{2+}) involved in the formation of insoluble corrosion films (such as MgO and $Mg(OH)_2$) on the surface of Mg. The potentiostat net current density (i_{net}) during anodic polarisation can be described by the summation of ICP determined Mg dissolution current density (i_{Mg}^{2+}), current density associated with the formation of corrosion films (i_{film}) and cathodic current density (i_c) [80, 81]:

$$i_{net} = i_{Mg}^{2+} + i_{film} - i_c \quad (2)$$

According to the Butler-Volmer equation, the cathodic current, i_c should decrease with the increasing potential during anodic polarisation, as larger anodic current is applied. In the case

of pure Mg, cathodic current however increases with increasing applied potential [20, 23, 26, 81]. Such a feature of cathodic activation is not readily tallied by conventional polarisation techniques (using potentiostat). In many cases, some electrons consumed by local cathodic reactions (such as those supported by corrosion films) might not be fully collected by the potentiostat [19, 20]. As such, similar values of i_{net} were obtained for the alloys prepared herein. In contrast, ICP determined dissolution current density (i_{Mg}^{2+}), was independent of the measured variation of cathodic current density during potentiodynamic polarisation, and is indicative of the relative kinetics of the anodic partial reaction ($Mg \rightarrow Mg^{2+}$).

To quantitatively assess the anodic kinetics of tested specimens, a $\frac{\Delta E}{\Delta I}$ slope fit was used to estimate potential dependent reaction kinetics as revealed by AESEC analysis (Fig. 8b). The $\frac{\Delta E}{\Delta I}$ slope was executed by the linear fit of ICP determined potentiodynamic polarisation results and shown in Table. 2.

It may be observed from the data in Table 2 that the ICP determined $\frac{\Delta E}{\Delta I}$ slope for Mg-Zn was slightly lower than that of pure Mg, suggesting that binary additions of Zn enhanced the rate of the anodic partial reaction. In contrast, the $\frac{\Delta E}{\Delta I}$ slope measured for Mg-Zn-Ge specimens increased with increasing ternary additions of Ge. An approximately 50% higher $\frac{\Delta E}{\Delta I}$ slope was obtained for Mg-1Zn-0.5Ge (wt.%) - compared to that of Mg-Zn alloys and pure Mg. This indicates the functionality of the combinations of Zn and Ge alloying to decrease the kinetics of the anodic partial reaction of Mg.

The assessment of cathodic activation by galvanostatic-potentiostatic experiments indicated that the rate of cathodic reaction sustained upon the surface of anodic polarised Mg-Zn-Ge alloys was significantly lower than that of pure Mg and Mg-Zn alloys. The custom-designed galvanostatic-potentiostatic electrochemical signals of experiments simulated the "on-off" cycles of Mg primary batteries in an aqueous environment. Parasitic discharge is a major issue in primary Mg battery system, where anodic dissolution (i.e. which occurs during the on or duty cycle) induces cathodic activation of Mg and subsequent enhanced Mg corrosion during the off (or no duty) cycle [19, 27, 29, 30]. The findings in the present work provide one possible means to produce more charge effective and durable Mg electrodes for primary aqueous batteries, although the quantification of any benefits would require a focused study.

Metallurgical additions of Zn and Ge additions reported herein achieved a similar outcome of corrosion control, as previously reported in Mg-As and Mg-Ge alloys [43, 45]. Furthermore, the Mg-Zn-Ge alloys displayed superior mechanical properties (~80 HV_1 and ~300 MPa yield strength) and appreciable ductility (~16-20 % elongation). Comparing the primitive property space of hardness/yield strength versus mass loss rate (which is a convincible and universal parameter to indicate corrosion rate of Mg) for the alloys produced herein with other types of Mg alloys is difficult. The reasons for this are on the basis that: (i) the mechanical property of Mg alloys is a complex function of corrosion resistance (which is generally revealed to be inversely correlated) [5, 31, 47, 48, 63]; (ii) a limited number of works to date simultaneously investigated the mechanical and corrosion property of Mg alloys [40, 47, 48, 63, 82]; whilst (iii) the study that carried out both types of testings in bio-simulated environment such as simulated body fluid (SBF) [6] is not of direct relevance for industry implications. The Mg-Zn-Ge alloys produced herein demonstrated simultaneously improved mechanical strength and corrosion resistance relative to both pure Mg and M-Zn alloy. The finding provides meaningful implications for the development of high strength and corrosion resistant Mg alloys.

The reduction of cathodic kinetics by combined alloying additions of Zn and Ge was ascribed to the ability of Ge to serve as a strong cathodic poison to hinder the kinetics of HER on the surface of cathodic sites of Mg. Cathodic activation and corrosion of Mg have been reported to be strongly correlated with Fe impurity level of Mg by McNulty and Hanawalt in 1942 [36, 37]. The tolerance limit of Fe has been determined to be ~170 ppm, above which the corrosion rate of Mg will increase dramatically [37, 83, 84]. The presence of Fe particles and Fe rich phase upon corroded Mg surface have been validated by several independent studies [24, 85-88]. The extent of cathodic activation of Mg has also been shown to vary as a function of Fe impurity concentration [22, 27, 80]. It is, therefore, plausible that Fe and Fe rich phase were important sites that support HER and cathodic activation of Mg. The kinetics of HER at the surface of Fe and many steels have been shown to be significantly retarded by absorption of cathodic poisons (such as arsenic, antimony, bismuth and tin) which reduced surface coverage of hydrogen atom intermediate (H_{ad}) and restricted hydrogen atom recombination towards HER [89-93]. It is thus postulated that the metallurgically alloyed Ge as explored in this study may also have a similar "cathodic poisoning" effect upon impurities or local cathode sites. The rationale is that since Ge has a 'noble' electrode potential of ~ +0.12 V_{SHE} [10], Ge and Ge containing phase are cathodically polarised during OCP and potentiodynamic

polarisation exposure of Mg (and Mg-alloys). Such apparently inert Ge containing particles may accumulate on the Mg-alloy matrix during anodic dissolution or are possibly dislodged and redeposited at local cathode sites [83, 85-88]. It is thus reasonable to hypothesise that Ge additions in the context of the ternary alloys studied herein, also serves to impart a cathodic poisoning effect that markedly suppresses cathodic kinetics [22, 35, 42, 43].

A recent study by Lysne, et al. investigated the cathodic activation of Mg samples with a range of Fe content ranging from 25 ppmw to 13000 ppmw [94]. A primitive model for cathodic activation was proposed based on the enrichment of Fe impurities alone, and it was suggested that efficiency of Fe enrichment upon anodic polarised Mg surface was low (less than 1%) [94]. In other works, cathodic activation was still reported to be manifested on the surface of ultra-high purity Mg (0.1 ppmw Fe) following anodic polarisation [80, 95]. Thus, Fe impurities are unlikely to be the only (or the major) factor that accounts for the cathodic activation of Mg in unalloyed Mg. Several independent studies showed that the formation of $Mg(OH)_2$ on the surface of Mg is also an important factor that contributed to the cathodic activation of Mg [9, 28, 81, 96-98]. A more recent density function theory (DFT) based study revealed that dilute additions of cathodic poison, such as As, Sb and Ge decreased the thermodynamic favourability of Mg (0001) surface of Mg slab model (with basal texture) towards HER [99]. Therefore, combined alloying additions of Zn and Ge used herein might also affect the formation of any surface hydroxide film which correspondingly hinders cathodic activation of Mg. This latter concept was very recently demonstrated as a feasible assumption from results obtained via DFT calculated equilibrium diagrams [100].

4 Conclusions

In the present work, Mg alloys with low-level additions of Zn (1 wt. %) and Ge (at 0.3 and 0.5 wt.%) were subjected to a range of testing to assess the electrochemical and mechanical properties of the prepared alloys. The following key conclusions may be drawn:

- The binary addition of Zn to Mg led to enhanced cathodic kinetics and more severe corrosion of pure Mg in the case of the extruded Mg-Zn alloys studied herein. However, metallurgical additions of Ge to Mg-Zn alloys were successfully able to offset the effects of Zn alloying by significantly decreasing the net cathodic (HER) kinetics in the case of Mg-Zn-Ge alloys relative to both Mg-Zn and pure Mg.
- The Mg-Zn-Ge alloy displayed remarkable corrosion resistance relative to both Mg-Zn and pure Mg, as indicated by both the mass loss and hydrogen collection tests. Concomitantly, the corrosion morphology in the case of alloys with Ge additions, was altered from a heavily corroded filiform-like corrosion attack to discrete superficial corrosion sites.
- The cyclic potentiostatic-galvanostatic tests indicated that the Mg-Zn-Ge alloys exhibited suppressed cathodic kinetics following prior anodic polarisation, in contrast to results of pure Mg and Mg-Zn alloys (both of which revealed evidence of classical cathodic activation). Such a result has ramifications in the case of Mg electrodes for use in aqueous primary battery systems.
- Results from AESEC testing were able to confirm the rankings of corrosion rate (from other methods). However, of significance, AESEC results also uniquely revealed that combined Zn and Ge alloying additions reduced the partial anodic dissolution rate of Mg.
- In addition to beneficial effects in the context of corrosion, combined Zn and Ge additions notably increased the hardness and yield strength of the Mg alloys reported herein. Such findings provide a practical means of improving both mechanical strength and corrosion resistance of Mg alloys (noting in the present case, an extruded alloy was presented). The combination of the strength reported, and low corrosion rate reported, is unique in the context of Mg-alloys to date, and as such represents an important breakthrough.

Acknowledgements

We acknowledge the use of facilities in the Monash Centre for Electron Microscopy. RLL is supported by a Monash Graduate Scholarship and Faculty of Engineering International Postgraduate Research Scholarship. NB is supported by Woodside Energy. JRS is supported by a DOE EFRC under Award # DE-SC0016584.

Reference:

[1] I.J. Polmear, Light alloys: metallurgy of the light metals, 3rd ed., Arnold, London, 1995.
[2] H. Baker, M.M. Avedesian, ASM International. Handbook Committee., Magnesium and magnesium alloys, ASM International, Materials Park, OH, 1999.
[3] J. Nie, Physical Metallurgy of Light Alloys, in: D.E.L. Hono (Ed.) Physical Metallurgy (Fifth Edition), Elsevier, Oxford, 2014, pp. 2009-2156.
[4] T.B. Abbott, Magnesium: Industrial and Research Developments Over the Last 15 Years, Corrosion, 71 (2015) 120-127.
[5] M. Esmaily, J.E. Svensson, S. Fajardo, N. Birbilis, G.S. Frankel, S. Virtanen, R. Arrabal, S. Thomas, L.G. Johansson, Fundamentals and advances in magnesium alloy corrosion, Progress in Materials Science, 89 (2017) 92-193.
[6] N.T. Kirkland, J. Lespagnol, N. Birbilis, M.P. Staiger, A survey of bio-corrosion rates of magnesium alloys, Corrosion Science, 52 (2010) 287-291.
[7] Y.F. Ding, R.W. Li, M. Nakai, T. Majumdar, D.H. Zhang, M. Niinomi, N. Birbilis, P.N. Smith, X.B. Chen, Osteoanabolic Implant Materials for Orthopedic Treatment, Advanced healthcare materials, 5 (2016) 1740-1752.
[8] T. Cain, L.G. Bland, N. Birbilis, J.R. Scully, A Compilation of Corrosion Potentials for Magnesium Alloys, Corrosion, 70 (2014) 1043-1051.
[9] T.W. Cain, M.A. Melia, J.M. Fitz-Gerald, J.R. Scully, Evaluation of the Potential Range for Sacrificial Mg Anodes for the Cathodic Protection of Mg Alloy AZ31B-H24, Corrosion, 73 (2017) 544-562.
[10] A.J. Bard, J.A.A. Ketelaar, Encyclopedia of Electrochemistry of the Elements, Journal of The Electrochemical Society, 121 (1974) 212C.
[11] G.L. Makar, J. Kruger, Corrosion of magnesium, International Materials Reviews, 38 (1993) 138-153.
[12] L.D. Chen, J.K. Nørskov, A.C. Luntz, Theoretical Limits to the Anode Potential in Aqueous Mg–Air Batteries, The Journal of Physical Chemistry C, 119 (2015) 19660-19667.
[13] P. Saha, M.K. Datta, O.I. Velikokhatnyi, A. Manivannan, D. Alman, P.N. Kumta, Rechargeable magnesium battery: Current status and key challenges for the future, Progress in Materials Science, 66 (2014) 1-86.
[14] W.J. Joost, P.E. Krajewski, Towards magnesium alloys for high-volume automotive applications, Scripta Materialia, 128 (2017) 107-112.
[15] M. Easton, S. Zhu, M. Gibson, T. Abbott, H.Q. Ang, X. Chen, N. Birbilis, G. Savage, Performance Evaluation of High-Pressure Die-Cast Magnesium Alloys, in: K.N. Solanki, D. Orlov, A. Singh, N.R. Neelameggham (Eds.) Magnesium Technology 2017, Springer International Publishing, Cham, 2017, pp. 123-129.
[16] A.A. Luo, Magnesium Development as a Lightweight Material—In Competition with Other Structural Materials, in: K.N. Solanki, D. Orlov, A. Singh, N.R. Neelameggham (Eds.) Magnesium Technology 2017, Springer International Publishing, Cham, 2017, pp. 7-7.
[17] D.A. Jones, Principles and prevention of corrosion, 2nd ed., Prentice Hall, Upper Saddle River, NJ, 1996.
[18] M. Pourbaix, Atlas of electrochemical equilibria in aqueous solutions, 2nd English ed., National Association of Corrosion Engineers, Houston, Tex., 1974.
[19] S. Thomas, N.V. Medhekar, G.S. Frankel, N. Birbilis, Corrosion mechanism and hydrogen evolution on Mg, Current Opinion in Solid State and Materials Science, 19 (2014) 85-94.
[20] G.S. Frankel, A. Samaniego, N. Birbilis, Evolution of hydrogen at dissolving magnesium surfaces, Corrosion Science, 70 (2013) 104-111.
[21] R.L. Liu, S. Thomas, J.R. Scully, G. Williams, N. Birbilis, An experimental survey of the cathodic activation of metals including Mg, Sc, Gd, La, Al, Sn, Pb and Ge in dilute chloride solutions of varying pH, Corrosion, (2017) 469-505.
[22] G. Williams, N. Birbilis, H.N. McMurray, Controlling factors in localised corrosion morphologies observed for magnesium immersed in chloride containing electrolyte, Faraday discussions, 180 (2015) 313-330.

[23] W. Beetz, On the development of hydrogen from the anode, Philosophical Magazine Series 32 (1866) 269-278.
[24] N. Birbilis, A.D. King, S. Thomas, G.S. Frankel, J.R. Scully, Evidence for Enhanced Catalytic Activity of Magnesium arising from Anodic Dissolution, Electrochimica Acta, 132 (2014) 277-283.
[25] G. Williams, H.N. McMurray, Localized Corrosion of Magnesium in Chloride-Containing Electrolyte Studied by a Scanning Vibrating Electrode Technique, Journal of the Electrochemical Society, 155 (2008) C340.
[26] N.T. Kirkland, G. Williams, N. Birbilis, Observations of the galvanostatic dissolution of pure magnesium, Corrosion Science, 65 (2012) 5-9.
[27] S. Thomas, O. Gharbi, S.H. Salleh, P. Volovitch, K. Ogle, N. Birbilis, On the effect of Fe concentration on Mg dissolution and activation studied using atomic emission spectroelectrochemistry and scanning electrochemical microscopy, Electrochimica Acta, 210 (2016) 271-284.
[28] T.W. Cain, I. Gonzalez-Afanador, N. Birbilis, J.R. Scully, The Role of Surface Films and Dissolution Products on the Negative Difference Effect for Magnesium: Comparison of Cl^- versus Cl^- Free Solutions, Journal of The Electrochemical Society, 164 (2017) C300-C311.
[29] F.W. Richey, B.D. McCloskey, A.C. Luntz, Mg Anode Corrosion in Aqueous Electrolytes and Implications for Mg-Air Batteries, Journal of The Electrochemical Society, 163 (2016) A958-A963.
[30] L. Yin, X. Huang, H. Xu, Y. Zhang, J. Lam, J. Cheng, J.A. Rogers, Materials, designs, and operational characteristics for fully biodegradable primary batteries, Advanced materials, 26 (2014) 3879-3884.
[31] K. Gusieva, C.H.J. Davies, J.R. Scully, N. Birbilis, Corrosion of magnesium alloys: the role of alloying, International Materials Reviews, 60 (2015) 169-194.
[32] L.G. Bland, A.D. King, N. Birbilis, J.R. Scully, Assessing the Corrosion of Commercially Pure Magnesium and Commercial AZ31B by Electrochemical Impedance, Mass-Loss, Hydrogen Collection, and Inductively Coupled Plasma Optical Emission Spectrometry Solution Analysis, Corrosion, 71 (2015) 128-145.
[33] A.D. Südholz, N. Birbilis, C.J. Bettles, M.A. Gibson, Corrosion behaviour of Mg-alloy AZ91E with atypical alloying additions, Journal of Alloys and Compounds, 471 (2009) 109-115.
[34] N. Birbilis, M.A. Easton, A.D. Sudholz, S.M. Zhu, M.A. Gibson, On the corrosion of binary magnesium-rare earth alloys, Corrosion Science, 51 (2009) 683-689.
[35] J.O.M. Bockris, B.E. Conway, Studies in hydrogen overpotential. The effect of catalytic poisons at platinized platinum and nickel, Transactions of the Faraday Society, 45 (1949) 989-999.
[36] J.D. Hanawalt, C.E. Nelson, J.A. Peloubet, Corrosion studies of magnesium and its alloys Trans AIME, 147 (1942) 273-299.
[37] R.E. McNulty, J.D. Hanawalt, Some Corrosion Characteristics of High Purity Magnesium Alloys, Transactions of The Electrochemical Society, 81 (1942) 423-433.
[38] A.D. Südholz, N.T. Kirkland, R.G. Buchheit, N. Birbilis, Electrochemical Properties of Intermetallic Phases and Common Impurity Elements in Magnesium Alloys, Electrochemical and Solid-State Letters, 14 (2011) C5.
[39] A. Samaniego, K. Gusieva, I. Llorente, S. Feliu, N. Birbilis, Exploring the possibility of protective surface oxides upon Mg alloy AZ31 via lutetium additions, Corrosion Science, 89 (2014) 101-110.
[40] W. Xu, N. Birbilis, G. Sha, Y. Wang, J.E. Daniels, Y. Xiao, M. Ferry, A high-specific-strength and corrosion-resistant magnesium alloy, Nature materials, 14 (2015) 1229-1235.
[41] L. Hou, M. Raveggi, X.B. Chen, W. Xu, K.J. Laws, Y. Wei, M. Ferry, N. Birbilis, Investigating the Passivity and Dissolution of a Corrosion Resistant Mg-33at.%Li Alloy in Aqueous Chloride Using Online ICP-MS, Journal of The Electrochemical Society, 163 (2016) C324-C329.
[42] D. Eaves, G. Williams, H.N. McMurray, Inhibition of self-corrosion in magnesium by poisoning hydrogen recombination on iron impurities, Electrochimica Acta, 79 (2012) 1-7.
[43] N. Birbilis, G. Williams, K. Gusieva, A. Samaniego, M.A. Gibson, H.N. McMurray, Poisoning the corrosion of magnesium, Electrochemistry Communications, 34 (2013) 295-298.
[44] G. Williams, H.A.-L. Dafydd, H.N. McMurray, N. Birbilis, The influence of arsenic alloying on the localised corrosion behaviour of magnesium, Electrochimica Acta, 219 (2016) 401-411.

[45] R.L. Liu, M.F. Hurley, A. Kvryan, G. Williams, J.R. Scully, N. Birbilis, Controlling the corrosion and cathodic activation of magnesium via microalloying additions of Ge, Scientific reports, 6 (2016) 28747.
[46] J. McDonald, Magnesium Base Alloy, in, Dow Chemical Co, 1942.
[47] X. Xia, J.F. Nie, C.H.J. Davies, W.N. Tang, S.W. Xu, N. Birbilis, The Influence of Low Levels of Zinc, Calcium, Gadolinium, Strontium, and Zirconium on the Corrosion of Magnesium for Wrought Applications, Corrosion, 71 (2015) 1370-1386.
[48] X. Xia, C.H.J. Davies, J.F. Nie, N. Birbilis, Influence of Composition and Processing on the Corrosion of Magnesium Alloys Containing Binary and Ternary Additions of Zinc and Strontium, Corrosion, 71 (2015) 38-49.
[49] Y. Song, E.-H. Han, D. Shan, C.D. Yim, B.S. You, The effect of Zn concentration on the corrosion behavior of Mg–xZn alloys, Corrosion Science, 65 (2012) 322-330.
[50] X. Gu, Y. Zheng, Y. Cheng, S. Zhong, T. Xi, In vitro corrosion and biocompatibility of binary magnesium alloys, Biomaterials, 30 (2009) 484-498.
[51] X.-B. Liu, D.-Y. Shan, Y.-W. Song, E.-H. Han, Effects of heat treatment on corrosion behaviors of Mg-3Zn magnesium alloy, Transactions of Nonferrous Metals Society of China, 20 (2010) 1345-1350.
[52] S. Zhang, X. Zhang, C. Zhao, J. Li, Y. Song, C. Xie, H. Tao, Y. Zhang, Y. He, Y. Jiang, Y. Bian, Research on an Mg-Zn alloy as a degradable biomaterial, Acta Biomater, 6 (2010) 626-640.
[53] S. Zhang, J. Li, Y. Song, C. Zhao, X. Zhang, C. Xie, Y. Zhang, H. Tao, Y. He, Y. Jiang, Y. Bian, In vitro degradation, hemolysis and MC3T3-E1 cell adhesion of biodegradable Mg–Zn alloy, Materials Science and Engineering: C, 29 (2009) 1907-1912.
[54] S. Cai, T. Lei, N. Li, F. Feng, Effects of Zn on microstructure, mechanical properties and corrosion behavior of Mg–Zn alloys, Materials Science and Engineering: C, 32 (2012) 2570-2577.
[55] R.-C. Zeng, J. Zhang, W.-J. Huang, W. Dietzel, K.U. Kainer, C. Blawert, W. Ke, Review of studies on corrosion of magnesium alloys, Transactions of Nonferrous Metals Society of China, 16 (2006) s763-s771.
[56] C.J. Boehlert, K. Knittel, The microstructure, tensile properties, and creep behavior of Mg–Zn alloys containing 0–4.4wt.% Zn, Materials Science and Engineering: A, 417 (2006) 315-321.
[57] A. Das, G. Liu, Z. Fan, Investigation on the microstructural refinement of an Mg–6wt.% Zn alloy, Materials Science and Engineering: A, 419 (2006) 349-356.
[58] X. Gao, J.F. Nie, Characterization of strengthening precipitate phases in a Mg–Zn alloy, Scripta Materialia, 56 (2007) 645-648.
[59] J.B. Clark, Transmission electron microscopy study of age hardening in a Mg-5 wt.% Zn alloy, Acta Metallurgica, 13 (1965) 1281-1289.
[60] J.F. Nie, X. Gao, S.M. Zhu, Enhanced age hardening response and creep resistance of Mg–Gd alloys containing Zn, Scripta Materialia, 53 (2005) 1049-1053.
[61] Z.R. Zeng, Y.M. Zhu, S.W. Xu, M.Z. Bian, C.H.J. Davies, N. Birbilis, J.F. Nie, Texture evolution during static recrystallization of cold-rolled magnesium alloys, Acta Materialia, 105 (2016) 479-494.
[62] Z.R. Zeng, M.Z. Bian, S.W. Xu, C.H.J. Davies, N. Birbilis, J.F. Nie, Effects of dilute additions of Zn and Ca on ductility of magnesium alloy sheet, Materials Science and Engineering: A, 674 (2016) 459-471.
[63] X. Xia, J.F. Nie, C.H.J. Davies, W.N. Tang, S.W. Xu, N. Birbilis, An artificial neural network for predicting corrosion rate and hardness of magnesium alloys, Materials & Design, 90 (2016) 1034-1043.
[64] A. International, ASTM Standard G1-03, in: Standard Practice for Preparing, Cleaning, and Evaluating Corrosion Test Specimens, PA: ASTM International, West Conshohocken, 2011.
[65] S. Lebouil, O. Gharbi, P. Volovitch, K. Ogle, Mg dissolution in phosphate and chloride electrolytes: Insight into the mechanism of the negative difference effect, Corrosion, 71 (2015) 234-241.
[66] S. Lebouil, A. Duboin, F. Monti, P. Tabeling, P. Volovitch, K. Ogle, A novel approach to on-line measurement of gas evolution kinetics: Application to the negative difference effect of Mg in chloride solution, Electrochimica Acta, 124 (2014) 176-182.
[67] K. Ogle, Atomic emission spectroelectrochemistry: A new look at the corrosion, dissolution and passivation of complex materials, Corros. Mater., 37 (2012) 58-65.

[68] J. Światowska, P. Volovitch, K. Ogle, The anodic dissolution of Mg in NaCl and Na2SO4 electrolytes by atomic emission spectroelectrochemistry, Corrosion Science, 52 (2010) 2372-2378.
[69] J.L. Wang, R.L. Liu, T. Majumdar, S.A. Mantri, V.A. Ravi, R. Banerjee, N. Birbilis, A closer look at the in vitro electrochemical characterisation of titanium alloys for biomedical applications using in-situ methods, Acta Biomaterialia, (2017).
[70] A.A. Nayeb-Hashemi, J.B. Clark, ASM International., Phase diagrams of binary magnesium alloys, ASM International, Metals Park, Ohio, 1988.
[71] A.D. King, N. Birbilis, J.R. Scully, Accurate Electrochemical Measurement of Magnesium Corrosion Rates; a Combined Impedance, Mass-Loss and Hydrogen Collection Study, Electrochimica Acta, 121 (2014) 394-406.
[72] G. Williams, N. Birbilis, H.N. McMurray, The source of hydrogen evolved from a magnesium anode, Electrochemistry Communications, 36 (2013) 1-5.
[73] L. Rossrucker, K.J.J. Mayrhofer, G.S. Frankel, N. Birbilis, Investigating the Real Time Dissolution of Mg Using Online Analysis by ICP-MS, Journal of the Electrochemical Society, 161 (2014) C115-C119.
[74] R.L. Liu, J.R. Scully, G. Williams, N. Birbilis, Reducing the corrosion rate of magnesium via microalloying additions of group 14 and 15 elements, Electrochimica Acta, 260 (2018) 184-195.
[75] H.Y. Wang, Z.P. Yu, L. Zhang, C.G. Liu, M. Zha, C. Wang, Q.C. Jiang, Achieving high strength and high ductility in magnesium alloy using hard-plate rolling (HPR) process, Scientific reports, 5 (2015) 17100.
[76] V.A. Skripnyak, N.V. Skripnyak, E.G. Skripnyak, V.V. Skripnyak, Influence of grain size distribution on the mechanical behavior of light alloys in wide range of strain rates, 1793 (2017) 110001.
[77] C.A. Walton, H.J. Martin, M.F. Horstemeyer, W.R. Whittington, C.J. Horstemeyer, P.T. Wang, Corrosion stress relaxation and tensile strength effects in an extruded AZ31 magnesium alloy, Corrosion Science, 80 (2014) 503-510.
[78] B. Song, C. Wang, N. Guo, H. Pan, R. Xin, Improving Tensile and Compressive Properties of an Extruded AZ91 Rod by the Combined Use of Torsion Deformation and Aging Treatment, Materials, 10 (2017).
[79] X.N. Gu, W.R. Zhou, Y.F. Zheng, Y. Cheng, S.C. Wei, S.P. Zhong, T.F. Xi, L.J. Chen, Corrosion fatigue behaviors of two biomedical Mg alloys - AZ91D and WE43 - In simulated body fluid, Acta Biomater, 6 (2010) 4605-4613.
[80] S. Fajardo, C.F. Glover, G. Williams, G.S. Frankel, The Source of Anodic Hydrogen Evolution on Ultra High Purity Magnesium, Electrochimica Acta, 212 (2016) 510-521.
[81] L. Rossrucker, A. Samaniego, J.P. Grote, A.M. Mingers, C.A. Laska, N. Birbilis, G.S. Frankel, K.J.J. Mayrhofer, The pH Dependence of Magnesium Dissolution and Hydrogen Evolution during Anodic Polarization, Journal of the Electrochemical Society, 162 (2015) C333-C339.
[82] K. Gusieva, N. Birbilis, Development of Mg-Al-Zn alloys with enhanced toughness and durability, in, Monash University, 2014, pp. 243.
[83] S. Simanjuntak, M.K. Cavanaugh, D.S. Gandel, M.A. Easton, M.A. Gibson, N. Birbilis, The Influence of Iron, Manganese, and Zirconium on the Corrosion of Magnesium: An Artificial Neural Network Approach, Corrosion, 71 (2014) 199-208.
[84] M. Liu, G.-L. Song, Impurity control and corrosion resistance of magnesium–aluminum alloy, Corrosion Science, 77 (2013) 143-150.
[85] T. Cain, S.B. Madden, N. Birbilis, J.R. Scully, Evidence of the Enrichment of Transition Metal Elements on Corroding Magnesium Surfaces Using Rutherford Backscattering Spectrometry, Journal of the Electrochemical Society, 162 (2015) C228-C237.
[86] N. Birbilis, T. Cain, J.S. Laird, X. Xia, J.R. Scully, A.E. Hughes, Nuclear Microprobe Analysis for Determination of Element Enrichment Following Magnesium Dissolution, ECS Electrochemistry Letters, 4 (2015) C34-C37.
[87] M. Taheri, J.R. Kish, N. Birbilis, M. Danaie, E.A. McNally, J.R. McDermid, Towards a Physical Description for the Origin of Enhanced Catalytic Activity of Corroding Magnesium Surfaces, Electrochimica Acta, 116 (2014) 396-403.

[88] Z.P. Cano, M. Danaie, J.R. Kish, J.R. McDermid, G.A. Botton, G. Williams, Physical Characterization of Cathodically-Activated Corrosion Filaments on Magnesium Alloy AZ31B, Corrosion, 71 (2015) 146-159.
[89] E.G. Dafft, K. Bohnenkamp, H.J. Engell, ChemInform Abstract: Investigations of the hydrogen evolution kinetics and hydrogen absorption by iron electrodes during cathodic polarization, Chemischer Informationsdienst, 10 (1979).
[90] B.E. Conway, B.V. Tilak, Behavior and Characterization of Kinetically Involved Chemisorbed Intermediates in Electrocatalysis of Gas Evolution Reactions, 38 (1992) 1-147.
[91] B.E. Conway, G. Jerkiewicz, Thermodynamic and electrode kinetic factors in cathodic hydrogen sorption into metals and its relationship to hydrogen adsorption and poisoning, Journal of Electroanalytical Chemistry, 357 (1993) 47-66.
[92] J.M. Jaksic, N.M. Ristic, N.V. Krstajic, M.M. Jaksic, Electrocatalysis for hydrogen electrode reactions in the light of fermi dynamics and structural bonding FACTORS—I. individual electrocatalytic properties of transition metals, International Journal of Hydrogen Energy, 23 (1998) 1121-1156.
[93] S.Y. Qian, B.E. Conway, G. Jerkiewicz, Kinetic rationalization of catalyst poison effects on cathodic H sorption into metals: relation of enhancement and inhibition to H coverage, Journal of the Chemical Society, Faraday Transactions, 94 (1998) 2945-2954.
[94] D. Lysne, S. Thomas, M.F. Hurley, N. Birbilis, On the Fe Enrichment during Anodic Polarization of Mg and Its Impact on Hydrogen Evolution, Journal of the Electrochemical Society, 162 (2015) C396-C402.
[95] S. Fajardo, G.S. Frankel, Effect of impurities on the enhanced catalytic activity for hydrogen evolution in high purity magnesium, Electrochimica Acta, 165 (2015) 255-267.
[96] J.A. Yuwono, N. Birbilis, K.S. Williams, N.V. Medhekar, Electrochemical Stability of Magnesium Surfaces in an Aqueous Environment, The Journal of Physical Chemistry C, 120 (2016) 26922-26933.
[97] K.S. Williams, V. Rodriguez-Santiago, J.W. Andzelm, Modeling reaction pathways for hydrogen evolution and water dissociation on magnesium, Electrochimica Acta, 210 (2016) 261-270.
[98] S.H. Salleh, S. Thomas, J.A. Yuwono, K. Venkatesan, N. Birbilis, Enhanced hydrogen evolution on Mg $(OH)_2$ covered Mg surfaces, Electrochimica Acta, 161 (2015) 144-152.
[99] K.R. Limmer, K.S. Williams, J.P. Labukas, J.W. Andzelm, First Principles Modeling of Cathodic Reaction Thermodynamics in Dilute Magnesium Alloys, Corrosion, 73 (2017) 506-517.
[100] J.A. Yuwono, N. Birbilis, R. Liu, Q. Ou, Q. Bao, N.V. Medhekar, Aqueous Electrochemical Activity of the Mg Surface: The Role of Group 14 and 15 Microalloying Elements, Journal of The Electrochemical Society, 164 (2017) C918-C929.

Table 1. Composition (in wt. %) of samples tested herein. Compositions were independently an

Alloy	Mg	Zn	Ge	Al	Cu	Si	Fe	
Mg	Bal.	0.005	-	0.005	0.002	0.02	0.006	0
Mg-1Zn	Bal.	1	-	0.013	0.001	0.02	0.005	0
Mg-1Zn-0.3Ge	Bal.	1.01	0.27	0.011	0.001	0.02	0.005	0
Mg-1Zn-0.5Ge	Bal	1.03	0.52	0.011	0.001	0.02	0.004	0

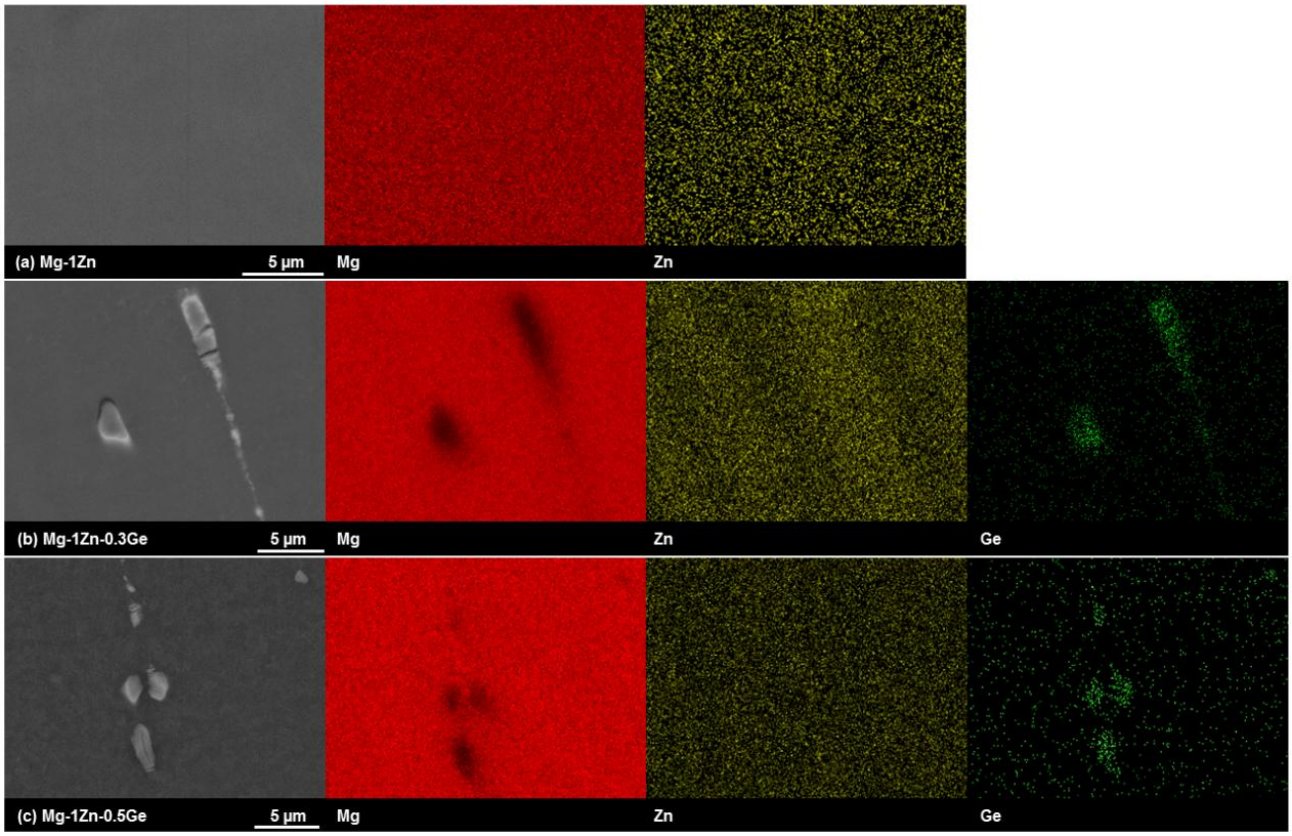

Figure. 1. Scanning electron micrographs in backscattered electron (BSE) mode, and corresponding EDX maps of Mg, Zn and Ge for the extruded alloys produced herein: (a) Mg-1Zn, (b) Mg-1Zn-0.3Ge and (c) Mg-1Zn-0.5Ge (wt.%).

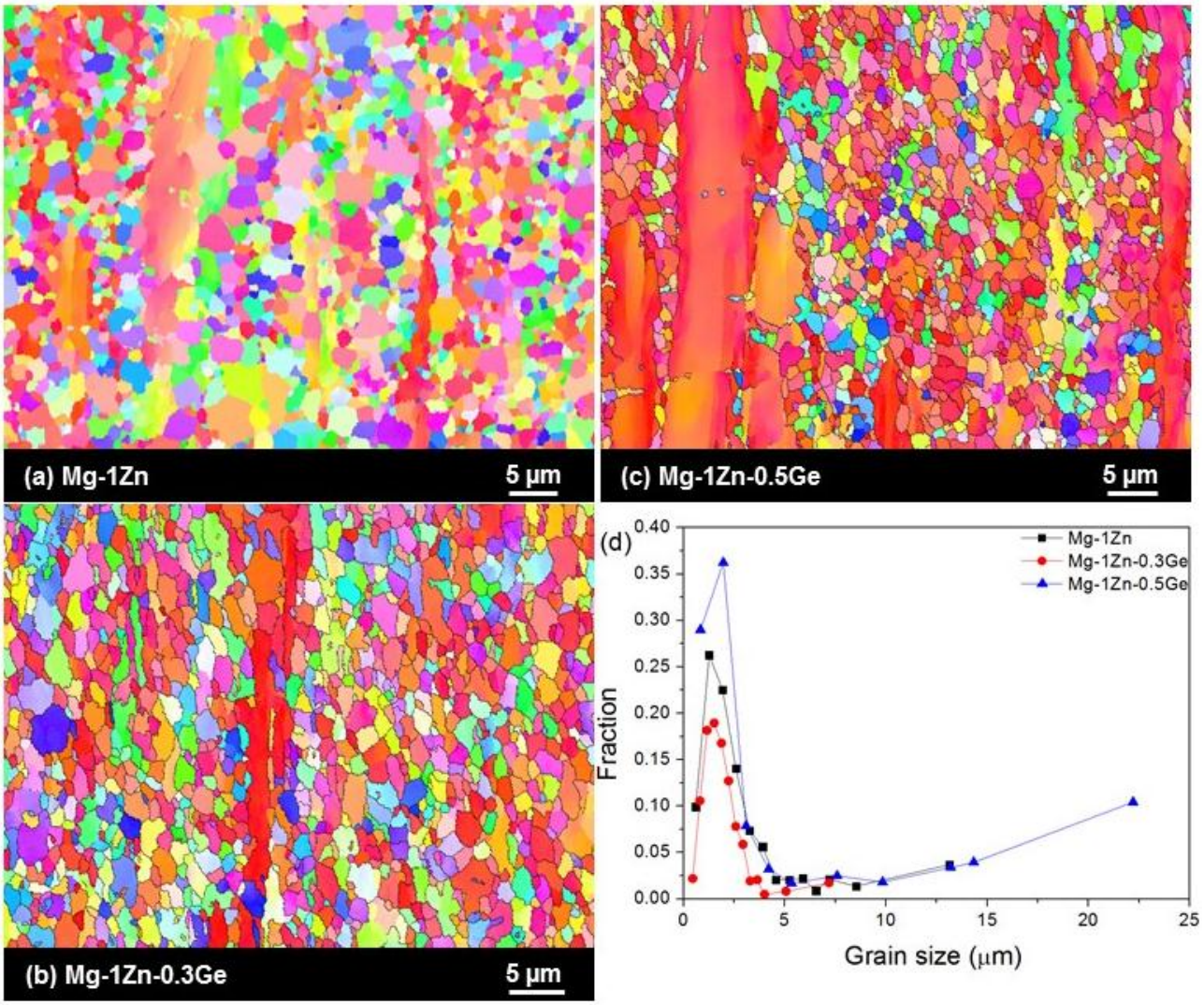

Figure. 2. EBSD maps of the extruded alloys produced herein: (a) Mg-1Zn, (b) Mg-1Zn-0.3Ge and (c) Mg-1Zn-0.5Ge (wt.%). (d) Grain size distribution of the custom prepared alloys. (Legend provides nominal alloy compositions in wt. %).

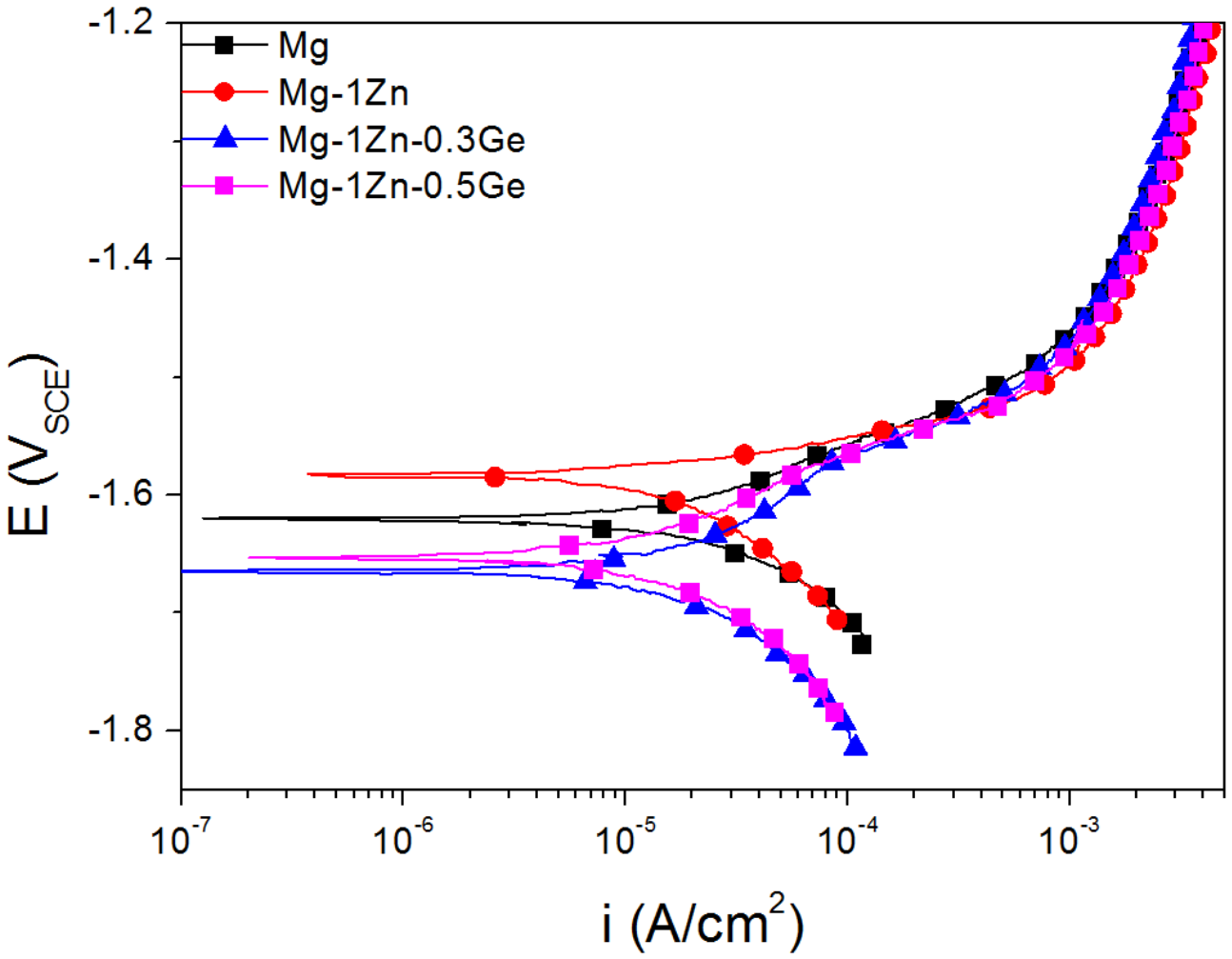

Figure. 3. Potentiodynamic polarisation in 0.1 M NaCl for Mg, Mg-1Zn, Mg-1Zn-0.3Ge and Mg-1Zn-0.5Ge extrusion alloys produced herein. Legend provides nominal alloy compositions in wt. %.

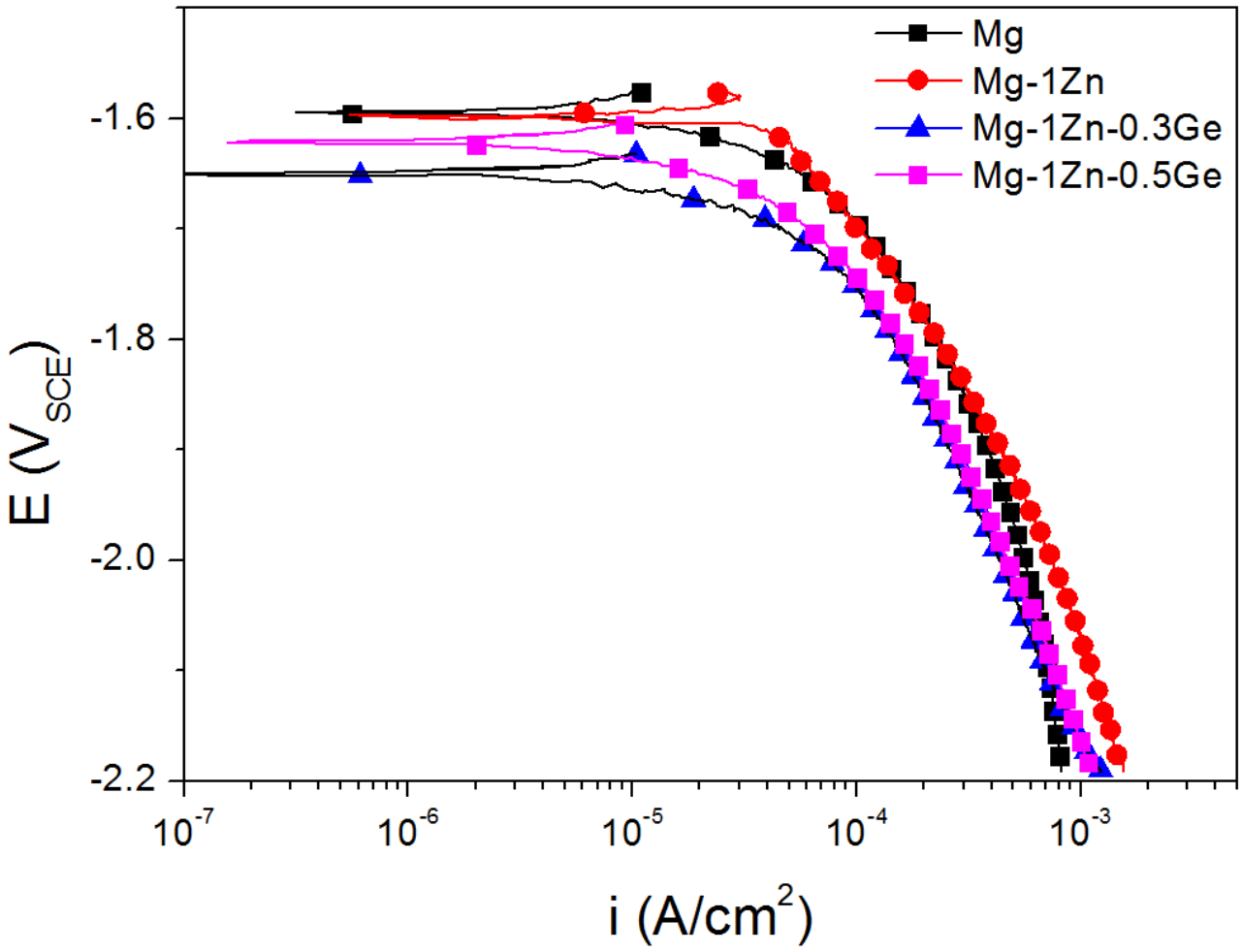

Figure. 4. Cathodic potentiodynamic polarisation response 0.1 M NaCl for Mg, Mg-1Zn, Mg-1Zn-0.3Ge and Mg-1Zn-0.5Ge extrusion alloys produced herein. Legend provides nominal alloy compositions in wt. %.

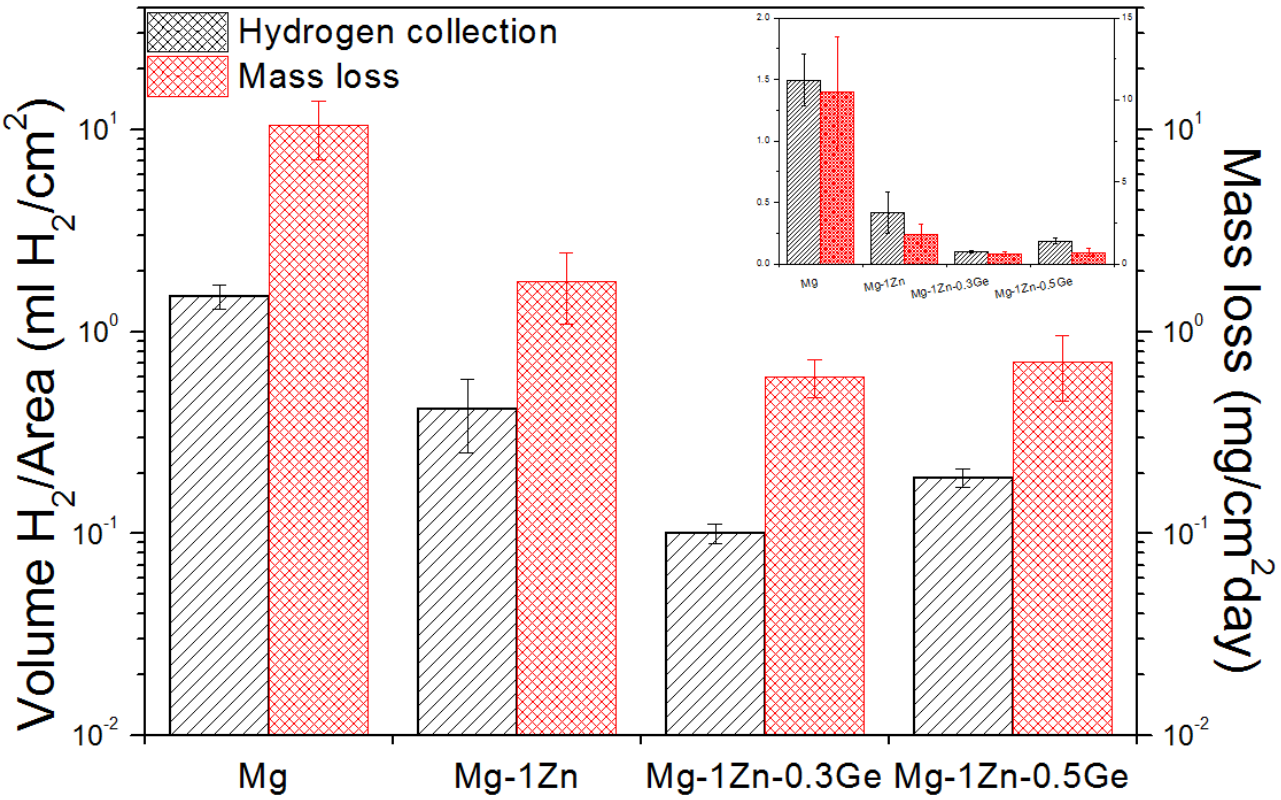

Figure. 5. Mass loss, and hydrogen collection, results for pure Mg and the Mg-1Zn, Mg-1Zn-0.3Ge and Mg-1Zn-0.5Ge extrusion alloys produced herein following 24 h immersion in 0.1 M NaCl. The nominal alloy compositions are provided in wt. % (inset displays results using a linear scale).

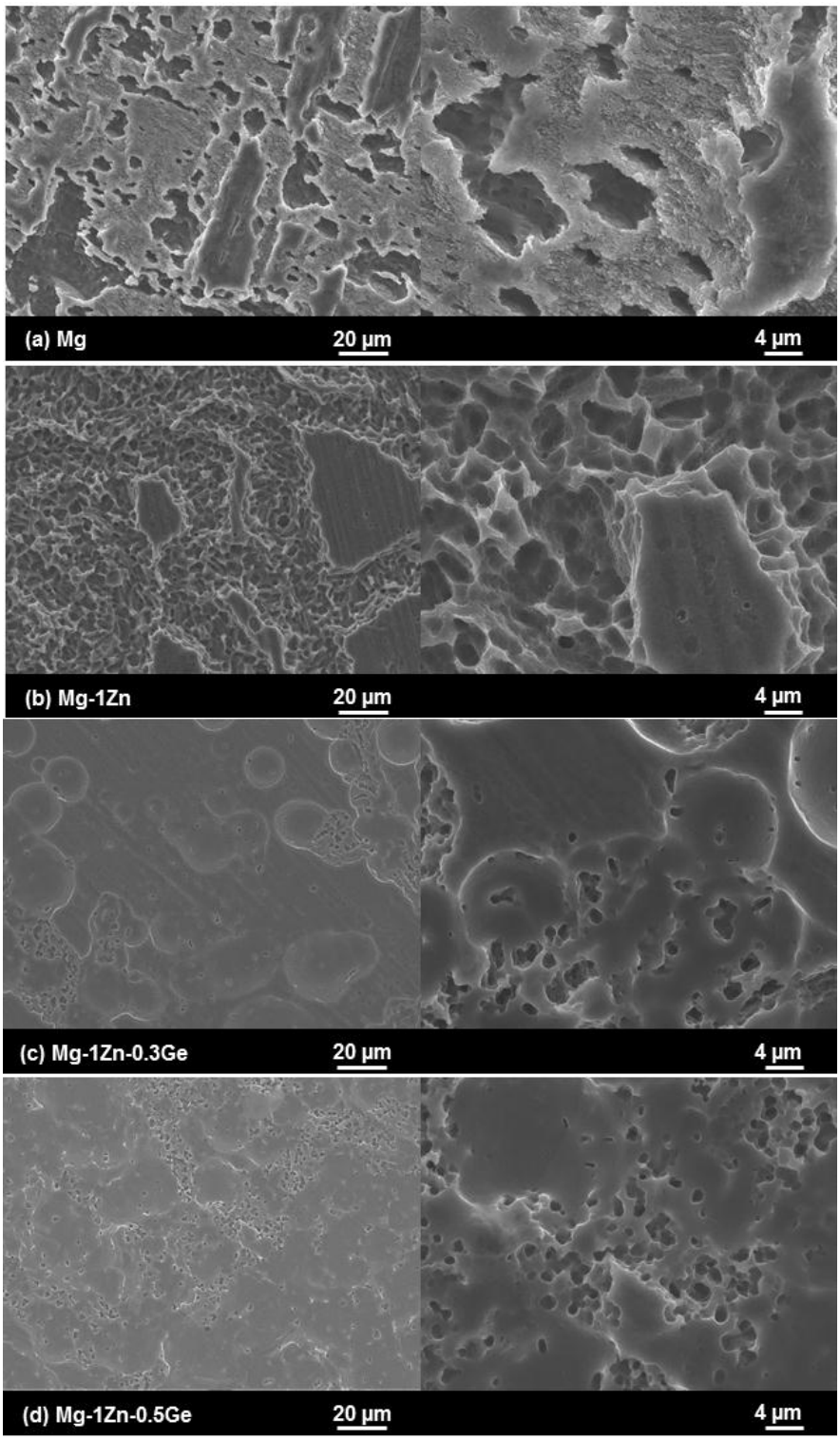

Figure. 6. Scanning electron micrographs in secondary electron (SE) mode of the surface morphology for: (a) Mg, (b) Mg-1Zn, (c) Mg-1Zn-0.3Ge and (d) Mg-1Zn-0.5Ge (wt.%) following 24 h immersion in 0.1 M NaCl. Images are presented at low (left) and high (right) magnification. Legend provides nominal alloy compositions in wt. %. Corrosion products were cleaned from sample surface using chromic acid solution (200 g/L chromium trioxide, 10 g/L silver nitrate and 20 g/L barium nitrate) to reveal the corrosion damage.

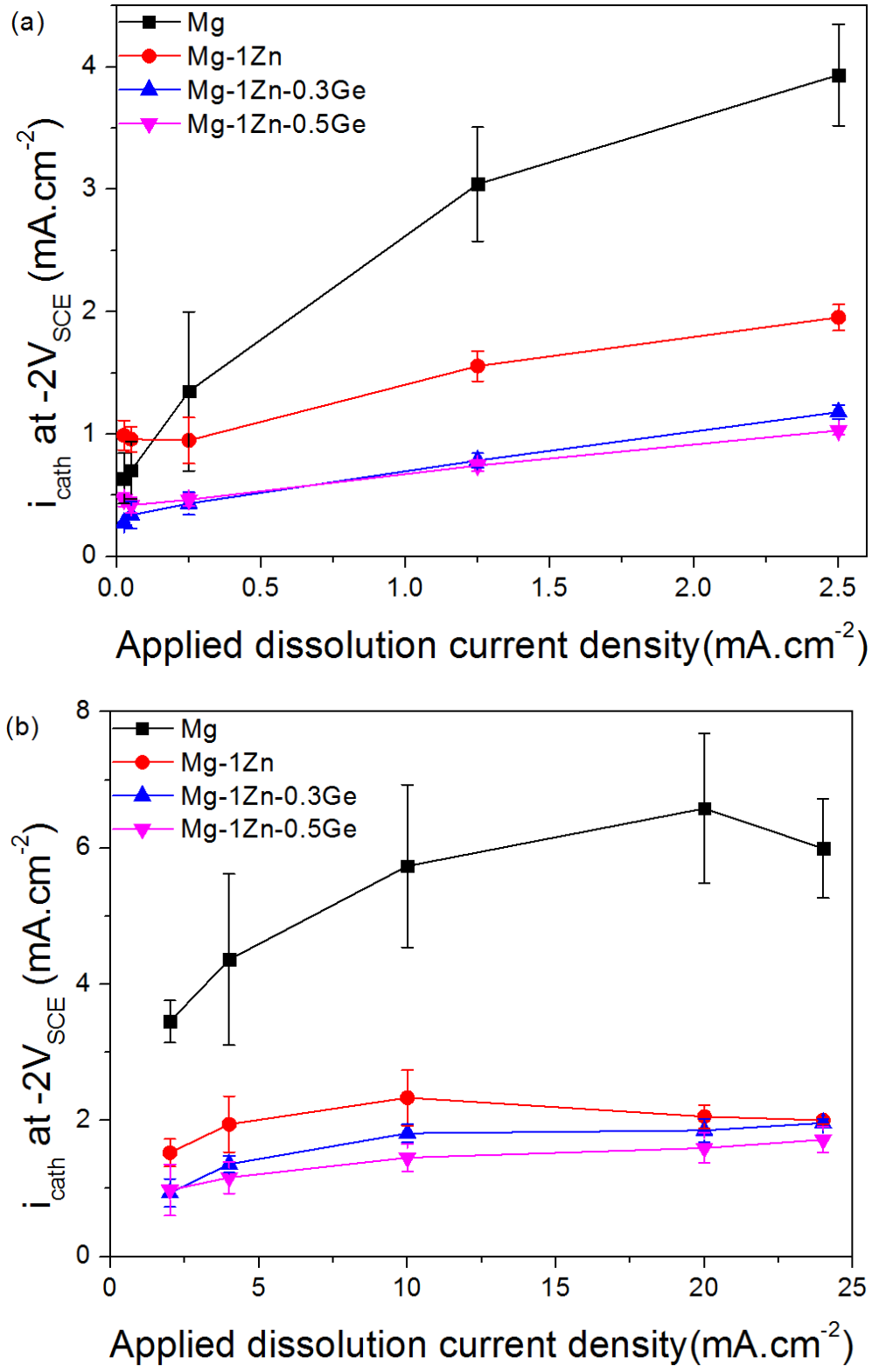

Figure. 7. Abridged results of measured cathodic current density at the fixed (cathodic) potential of -2.0 V_{SCE} in response to a prior anodic current signal, whereby the prior applied anodic current signals were: (a) 0.025 to 2.5 mA/cm^2 in a stepwise manner, and (b) 2 to 24 mA/cm^2 in a stepwise manner, for pure Mg and the Mg extrusion alloys produced herein in 0.1 M NaCl.

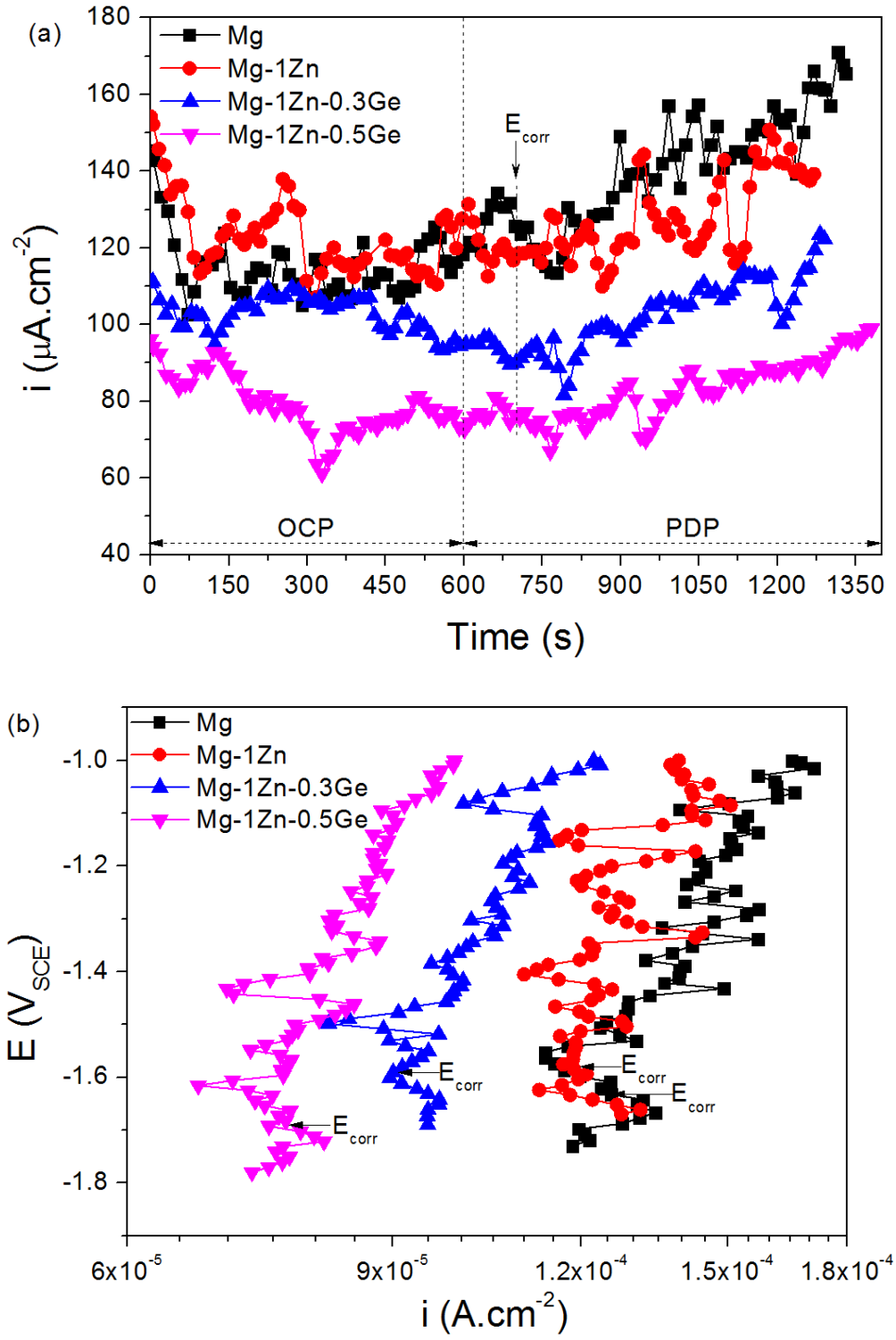

Figure. 8. (a) Current density i_{Mg}^{2+} determined by online ICP-OES analysis during the open circuit potential (OCP) and potentiodynamic polarisation (PDP) exposure for pure Mg and the Mg extrusion alloys produced herein in 0.1 M NaCl. Legend provides nominal alloy compositions in wt. %. (b) Potentiodynamic polarisation data presented in the format of applied potential vs. current density i_{Mg}^{2+} for pure Mg and the Mg alloys produced herein.

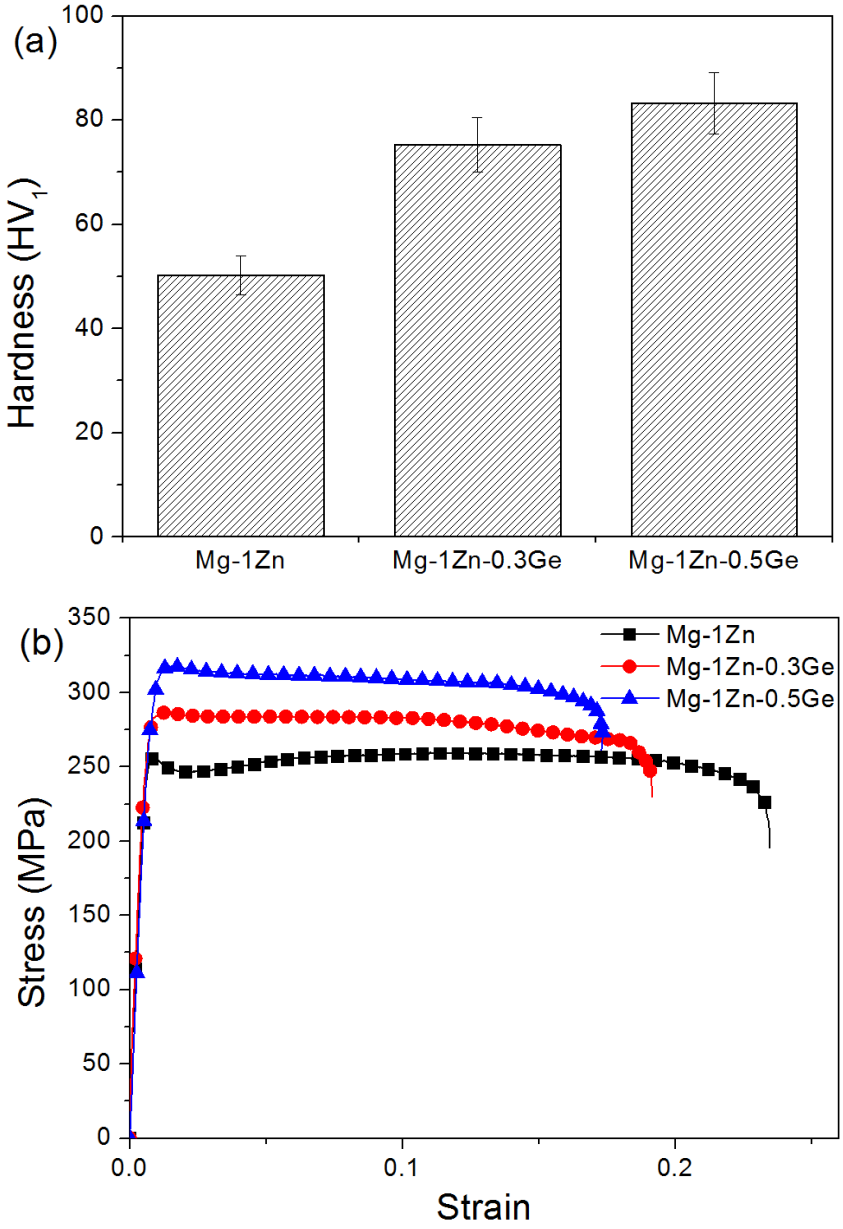

Figure. 9. (a) Microhardness of Mg-1Zn, Mg-1Zn-0.3Ge and Mg-1Zn-0.5Ge (wt.%). (b) Engineering stress strain curves of Mg-1Zn, Mg-1Zn-0.3Ge and Mg-1Zn-0.5Ge (wt.%). Legend provides nominal alloy compositions in wt. %.

Table 2. Summary of the ($\frac{\Delta E}{\Delta I}$) slope as determined during AESEC for pure Mg and the Mg extrusion alloys produced herein.

Alloy	ICP determined $\frac{\Delta E}{\Delta I}$ ($V/\mu A.cm^2$)
Mg	0.0114
Mg-1Zn	0.0106
Mg-1Zn-0.3Ge	0.0168
Mg-1Zn-0.5Ge	0.0234